

RESEARCH ARTICLE

Fire ants actively control spacing and orientation within self-assemblages

Paul C. Foster¹, Nathan J. Mlot¹, Angela Lin¹ and David L. Hu^{1,2,*}

ABSTRACT

To overcome obstacles and survive harsh environments, fire ants link their bodies together to form self-assemblages such as rafts, bridges and bivouacs. Such structures are examples of self-assembling and self-healing materials, as ants can quickly create and break links with one another in response to changes in their environment. Because ants are opaque, the arrangement of the ants within these three-dimensional networks was previously unknown. In this experimental study, we applied micro-scale computed tomography, or micro-CT, to visualize the connectivity, arrangement and orientation of ants within an assemblage. We identified active and geometric mechanisms that ants use to obtain favorable packing properties with respect to well-studied packing of inert objects such as cylinders. Ants use their legs to push against their neighbors, doubling their spacing relative to random packing of cylinders. These legs also permit active control of their orientation, an ability ants use to arrange themselves perpendicularly rather than in parallel. Lastly, we found an important role of ant polymorphism in promoting self-aggregation: a large distribution of ant sizes permits small ants to fit between the legs of larger ants, a phenomenon that increases the number of average connections per ant. These combined mechanisms lead to low packing fraction and high connectivity, which increase raft buoyancy and strength during flash floods.

KEY WORDS: Granular, Entanglement, Cooperative, Emergent, Packing

INTRODUCTION

Ants and bees link their bodies together to build self-assemblages such as curtains, rafts, bridges and bivouacs (Anderson et al., 2002; Cully and Seeley, 2004; Schneirla, 1971). Such assemblages perform functions similar to their counterparts in human architecture, but are built and maintained in a completely different manner. Self-assemblages can react to their environments, self-heal under environmental damage, and self-assemble using interchangeable parts without central control. Understanding how such structures are built may inspire similar feats with modular robotics and other synthetic materials (Groß and Dorigo, 2008).

The most significant barrier in characterizing self-assemblages is their opacity, which makes it impossible to measure the arrangement and connectivity of the network with the naked eye. Network properties such as connectivity have significant implications on the structure's strength, buoyancy and rate of construction, which in turn directly affect the survivability of the colony. In this investigation,

we employed micro-computed tomography (micro-CT) and scanning electron microscopy (SEM) to elucidate the network structure of a fire ant (*Solenopsis invicta* Buren) self-assemblage.

Anderson et al. coined the term self-assemblage for assemblies in which an individual is the building block for a variety of adaptable colony configurations (Anderson et al., 2002). Self-assemblages are often observed in a static state: individuals on the outside of the assemblages grip one another with legs or mandibles and remain in position until a specific task or goal is reached (Anderson et al., 2002; Lioni et al., 2001; Anderson and McShea, 2001). Colonies of fire ants can easily be observed building self-assemblages, such as a raft (Fig. 1A), hanging column (Fig. 1B), bivouac (Fig. 1C), an escape droplet (Fig. 1D) and tower (Fig. 1E). The dynamics of formation of the escape drop and the ant raft has been studied with great detail (Mlot et al., 2011; Bonabeau et al., 1998; Theraulaz et al., 2001), and we now understand how the motion of ants within these structures leads to their distribution of sizes and shapes.

The physical properties of ant assemblages have received very little attention. Indeed, in his review on self-assemblages, Anderson states: ‘virtually nothing is known regarding the... physical constraints these structures are under; these are the most important avenues for future research’ (Anderson et al., 2002). Mlot et al. found a variety of properties of fire ant rafts facilitating water travel (Mlot et al., 2011). Rafts are hydrophobic when linked, a property that keeps water from permeating the raft's underside when floating. They are buoyant, by virtue of their density of one-fifth that of water, which elicits a sizable restoring force if the raft is submerged. Mlot et al. also provided measurements of the strength and speed by which ant rafts are built. Ants can grip one another with a force 400 times their own weight. Despite the great strength holding the raft together, rafts can be built rather quickly: thousands of ants are able to rearrange themselves from a ball of ants to a two-layer stable raft in only 200 s. In this study, we provide a micro-structural context for how these attractive properties are maintained.

In studying the network structure of the ants, it is useful to view the aggregation as an active granular system, in which particles can sense their surroundings and adjust their bodies accordingly. A theory of active granular systems currently does not exist. In contrast, the study of inert granular particles, such as sand, nuts or medical pills, is an active area of research. Such granular materials are the second-most manipulated material in industry, and have attracted attention because they can appear both as liquids and as solids. This phase-change behavior is the focus of many experimental and computational studies to understand bulk properties (Donev et al., 2004). We review here the studies most amenable to comparison with ants.

In our study, we compared the actively constructed aggregations of ants to several control groups of granular particles. The first group is an aggregation of dead ants, which shows how ants would pack if they were not actively seeking connections with their legs.

¹School of Mechanical Engineering, Georgia Institute of Technology, Atlanta, GA 30332, USA. ²School of Biology, Georgia Institute of Technology, Atlanta, GA 30332, USA.

*Author for correspondence (hu@me.gatech.edu)

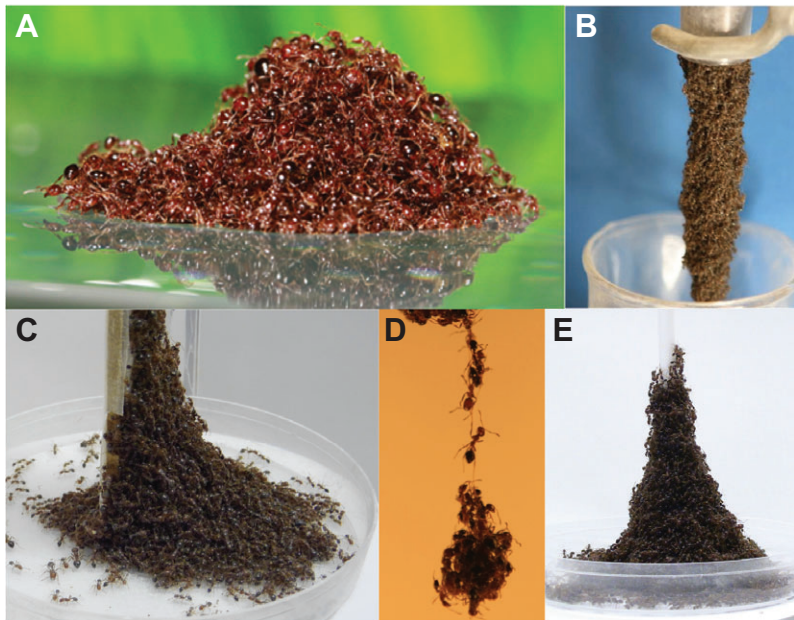


Fig. 1. Ant self-assemblages. (A) Raft, (B) hanging column, (C) bivouac, (D) escape droplet and (E) tower.

The second group is an aggregation of cylinders of the same aspect ratio α as the ants, giving insight into how legless ants would pack. This second system also falls under the class of prolate granular particles, which has been studied by several investigators. Desmond and Franklin showed that elongated particles, such as nails, cohere together into solids if their aspect ratio α is sufficiently high (Desmond and Franklin, 2006). Blouwolf and Fraden measured the distribution of the contact number c for randomly packed cylinders (Blouwolf and Fraden, 2006); in the Discussion (see ‘Highly inter-connected networks’), we compare these values with those exhibited by ants. Experimental limitations have motivated the use of simulations to predict critical packing parameters. Zhao et al. simulated spherocylinder packing of varying aspect ratio α and observed the effects on packing fraction ϕ and contact number c (Zhao et al., 2012). These studies, the results of which are re-printed in the Discussion (see ‘Ants maintain spacing using active pushing of their legs’), will provide insight into how ants improve their packing properties using both their behavior and their geometry.

This study also may shed light on the ability of biological systems to entangle. Entanglement is the ability of convex particles to interpenetrate one another and act cohesively. Gravish et al. studied the packing of staples, or U-shaped particles (Gravish et al., 2012). Using a plug of entangled staples, they elicited a phase transition from solid to liquid to gas by vibrating the plug, demonstrating that staple barb length is a key parameter for determining activation energy for this transition. Similar to staple barbs, ant legs penetrate the spaces around neighboring ants to increase connectivity. Also, like staple barbs, ant legs can occlude neighboring ants from filling nearby space, and so effectively reducing packing fraction relative to staples without their barbs.

In this study, we identified the key principles ants use to maintain favorable packing properties, and present a new methodology for generating 3D renderings of the self-assemblage and extracting quantitative data on the network of ants, including findings on ant connectivity, packing fraction, spacing and orientation within an assemblage. We also contextualize our results and discuss the implications of our findings, particularly with respect to biomaterials and the study of granular media.

RESULTS

SEM investigation

Ants can increase the strength of a structure by increasing their connectivity. Fig. 1B shows a funnel extruding a hanging column of ants with radius 12 mm supporting the weight of thousands of ants. Given an ant mass of 1 mg and a previously found planar packing density of 34 ants cm^{-2} (Mlot et al., 2011), we calculate that 150 ants at the exit of the funnel support 2000 of their neighbors hanging below them, indicating that each of the 150 ants is supporting the weight of 13 of their neighbors. They can remain in this configuration for 10 min or more. To investigate the source of this strength, SEM scans were used to qualitatively evaluate connection types, and then CT data to obtain bulk statistics of connections.

SEM imaging as shown in Fig. 2 reveals the different mechanisms ants use to stay connected in an assemblage. We employed SEM imaging because its magnification and resolution are much higher than those of CT imaging, making it useful in ascertaining the types of connections. SEM permits only ants on the surface of a self-aggregation to be observed, limiting the technique to small sample sizes. Thus, to obtain quantitative data on the connection types, we also used CT scanning (see ‘CT scans’ section).

Connection is maintained mostly by the tarsal segment of the ant, shown in isolation in Fig. 2A. Attachment is achieved through the dual use of both the claws, clearly seen, and the adhesive pad, visible in Fig. 2D between the claws. The most common attachment between ants is a tarsal connection seen in Fig. 2B,D. Here, the adhesive pad is used to adhere both to smooth ant body parts and to rough hairy surfaces. Adhesive pad to tarsal connections are the most common attachments found in ant assemblages. A simple experiment illustrates the importance of the adhesive pad relative to the claw in maintaining these connections. Coating ants in talcum powder dries out the sticky pad while still permitting hooking by claws. Consequently, talc-coated ants can neither climb smooth surfaces nor form self-aggregations, behaviors for which the adhesive pad is needed.

The least common attachment type is the use of mandibles to grasp neighbors as shown in Fig. 2C. Roughly 1 in 10 ants uses their mandibles to grasp a neighboring ant’s leg, accounting for about one out of every 60 connections. Mandible connections provide a much stronger connection to neighbors than that offered by a tarsal

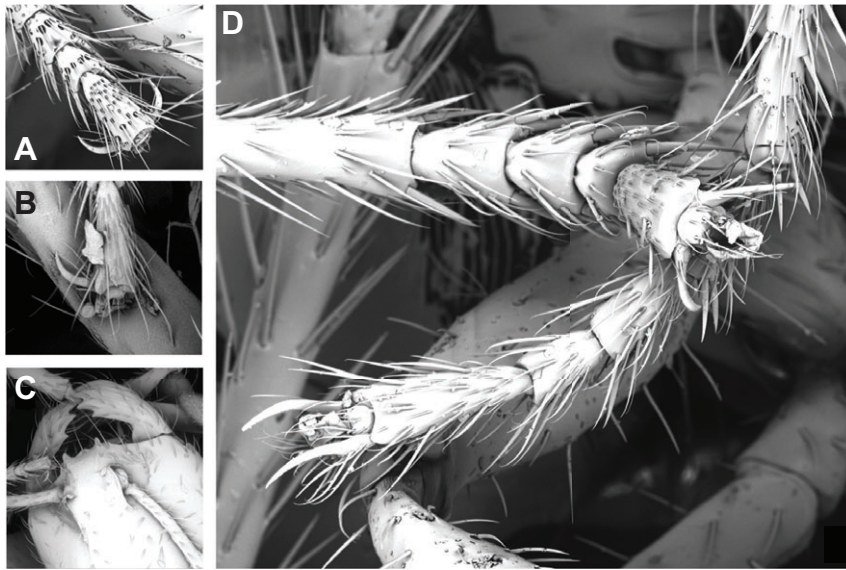


Fig. 2. Ants use legs and mandibles to form connections with neighbors. Here we show scanning electron microscopy images of (A) an ant tarsus, (B) a connection to a leg made using an adhesive pad, (C) a connection between a mandible and a leg, and (D) a connection involving both claws and adhesive pads.

connection; however, they are rare enough that we did not include them in our quantitative analysis.

CT scans

We employed methods of CT scanning to characterize the 3D network across a large numbers of ants. Fig. 3B is a representative rendering of 30 large ants illustrating the resolution obtainable through this method. In supplementary material Movie 1 we simultaneously pan through the CT scan cross-sections and the resulting 3D rendering. A typical scan comprises over 100 ants, and over 600 legs, which obscure the image. To more easily visualize the ant bodies for image processing, we used MATLAB to digitally remove ant legs. Fig. 3C shows a rendering of ants with legs removed, and color assignments to improve visualization of the arrangement and orientation of ants in an assemblage.

Connections and neighbors

In the context of granular media, connectivity is typically described by contact number c , defined as the number of contacts with an adjoining particle. However, measuring the connectivity of ants

requires new definitions because ants have both outgoing connections made by their own six legs and mandibles and incoming connections made by their neighbors' legs and mandibles, as shown in Fig. 4. Because mandible connections are exceedingly rare, we ignored them and considered only leg connections. We define c_{in} and c_{out} to be the number of incoming and outgoing connections, respectively, for a given ant. The total contact number, c_{total} , is defined as the sum of c_{out} and c_{in} : $c_{total} = c_{out} + c_{in}$.

An ant's neighbors are defined as the distinct ants connected to that ant via any connection. For convex particles the number of connected neighbors is always the same as the contact number c .

Fig. 5A and supplementary material Movie 2 show views of a single ant digitally isolated from the network. An ant is connected to its neighbors both by its own outgoing legs (c_{out}) highlighted in blue and incoming legs (c_{in}) highlighted in red. Fig. 5B is the distribution of the number of neighbors each ant shares, where the term neighbor is limited to ants with a structural connection. We found that on average each ant is connected to 4.8 neighbors.

As every ant has six legs, we defined the number of outgoing connections as $c_{out} = 6$, assuming every leg contacts a neighbor (see

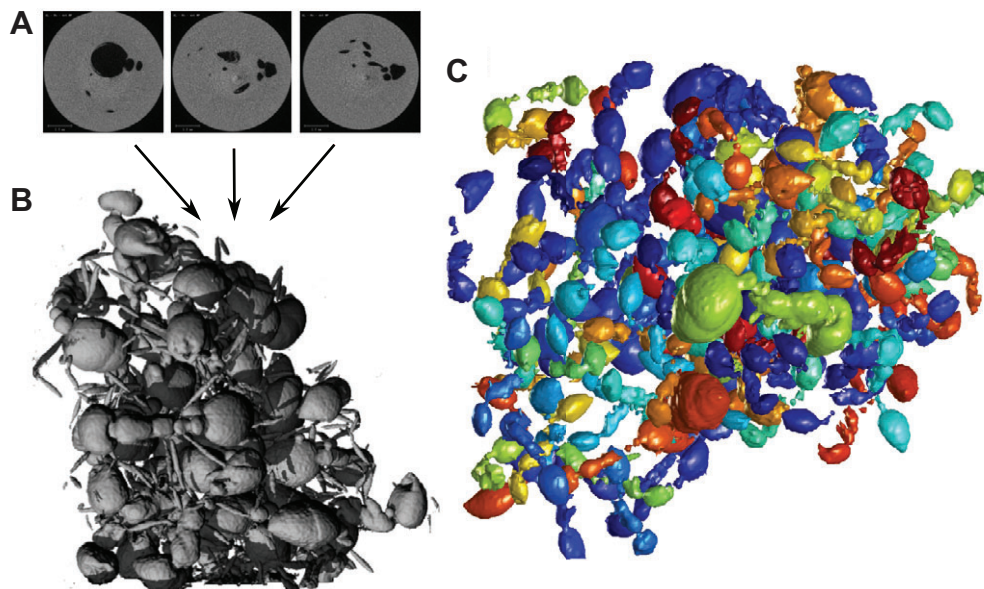


Fig. 3. Reconstructions of ant aggregations using micro-computed tomography (micro-CT). (A) Ant samples are scanned with a micro-CT scanner, producing thousands of 2D image layers. (B) These layers are stacked digitally to create 3D renderings of the connected ant network. This particular image was created by aggregating and then freezing 30 of the largest ants in a colony. (C) In another sample, ant legs were digitally removed to leave only ant bodies, which are then colored to more easily distinguish them.

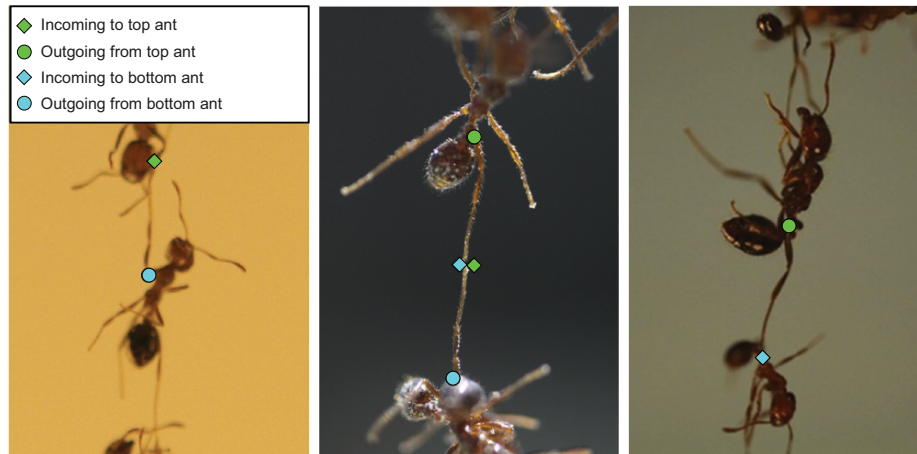


Fig. 4. Ant connections are recorded as incoming or outgoing relative to each ant. Here we show three photographic examples of ant connections separated from the rest of the aggregation, showing leg to head, leg to leg, and leg to body connections. An outgoing connection is any point where a connection leaves the body of the ant under consideration. An incoming connection is any point where a connection from another ant makes contact with the ant under consideration. As shown, this may involve a head, body or leg contact, and connections may be mutual, as in the middle image. Also note that the number of connections may not represent the number of physical contacts between ants; however, the case of tip to tip connections as shown in the middle panel usually only occurs when the ant aggregation is being pulled apart, so the number of connections is a close approximation to the number of physical contacts.

Materials and methods, ‘Calculation of measurements’ for justification). We measured the mean number of incoming connections as $c_{in}=8.25\pm 3.09$ (all measurements are reported as means \pm s.d. in the text and in Table 1). Thus each ant contacts its neighbors a total (c_{total}) of 14 times. This value is 40% higher than the maximum number for granular particles (Wouterse et al., 2007).

Fig. 5C shows the histogram of incoming connections c_{in} . We found that the number of connections can range rather widely, from 4 to 21. The minimum number of connections is associated with ants on the outside of the cluster, which are connected to fewer ants than those in the center.

Fig. 6D shows the relationship between ant body surface area and incoming connections for one of our samples. The trend fits a power

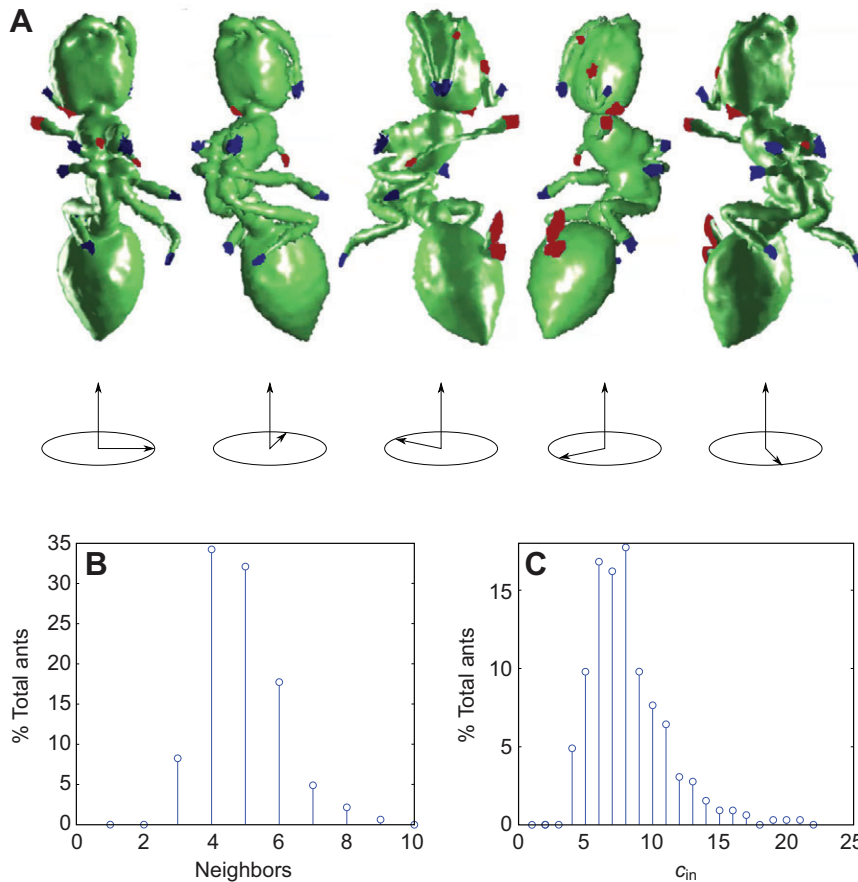


Fig. 5. Number of neighbors and connections. (A) Five views of a single ant in an assemblage. Blue highlights, whose number is equal to c_{out} , indicate outgoing connections (i.e. the ant’s own legs). Red highlights, whose number is equal to c_{in} , indicate the incident connecting legs from neighboring ants. View rotation angles are shown below. (B) Distribution of neighboring ants to which a single ant is connected. (C) Distribution of incoming connections, c_{in} , for each ant within a self-assemblage.

Table 1. Geometric and packing properties of ants in this study

| | <i>n</i> | ϕ | NND ₁₋₄ | <i>C</i> _{total} | Ψ |
|-----------|----------|-----------|--------------------|---------------------------|-----------|
| Live ants | 440 | 0.25±0.05 | 1.82±0.31 | 14.25±3.09 | 0.44±0.27 |
| Dead ants | 220 | 0.38±0.01 | 1.23±0.26 | NA | 0.60±0.28 |
| Cylinders | | 0.6 | | 9 | >0.5 |
| Staples | | 0.13 | | 8.7 | |

Both live and dead ants are provided for comparison. Results from studies of cylinders (Wouterse et al., 2007) and staples (Gravish et al., 2012) are provided to give perspective. Packing fraction ϕ is averaged from four live samples and from two dead samples. Nearest neighbor distance (NND), total connections (*C*_{total}) and orientation correlation (Ψ) are all averaged from 440 live ants and 220 dead ants. All measurements are reported as means ± s.d. For reference values, s.d.<0.01. Cylinder orientation was reported as a more parallel alignment, written here as >0.5. Connection count is not given for dead ants because of measurement difficulties described in Materials and methods (see 'Measurement difficulties in dead ant samples').

law with an exponent of 0.35 and R^2 value of 0.53. In comparison, Fig. 6C shows the relationship between ant body surface area and the number of neighbors, which fits a power law function with an exponent of 0.41 and R^2 of 0.44. This fit compares with our simulation of the packing of spheres of varying radius (see Materials and methods, 'Comparison with simulations'), which shows a power law with an exponent of 0.6 and R^2 of 0.99, as seen in Fig. 6C in red. This simulation indicates that the number of ant neighbors should not scale linearly with ant size. Moreover, the fit is similar to that observed for the number of ant neighbors, consistent with the hypothesis that polymorphism is responsible for a portion of the variation.

Nearest neighbor distance and packing fraction

We define the nearest neighbor distance NND₁ as the distance from an ant centroid to the nearest ant centroid, the second nearest neighbor distance NND₂ as the distance to the second nearest ant centroid, and so on. These numbers were compared between live and dead CT scanned samples to assess the ants' active control over spacing. For consistency with the literature, this metric does not take into account connectivity.

Live ants have a nearest neighbor distance, NND₁, of 0.99±0.25 mm, which is within 0.01 mm of the corresponding

value for dead ants. This result is surprising, given that the packing fraction is significantly lower for live ants, suggesting the ants should be further apart. Further investigation showed the expected change when the second to fourth nearest neighbors were included. The average of nearest neighbor NND₁ to NND₄ for live ants is 1.82±0.31 mm, which is 48% larger than that for dead ants (1.23±0.26 mm). The difference is statistically significant with $P<0.0001$ (nested ANOVA: $F_{1,4}=1417$, $F_{4,654}=0.4144$, $N_1=4\times 110$, $N_2=2\times 110$, variation between subgroups not significant at $\alpha=0.05$).

To compare packing of ants with that of other granular materials, it is useful to discuss packing fraction rather than the equivalent nearest neighbor distance. We define packing fraction for a sample of ants as:

$$\phi = \frac{\sum_{i=1}^n V_i}{V_{\text{total}}}, \quad (1)$$

where V_i is the volume of the *i*th ant and the numerator is summed over all *n* ants in a sample. V_{total} is the container volume, determined by using our software by dilating [a standard image processing operation described, for example, by Haralick (Haralick, 1992)] the ant ball until 95% of the interior is filled.

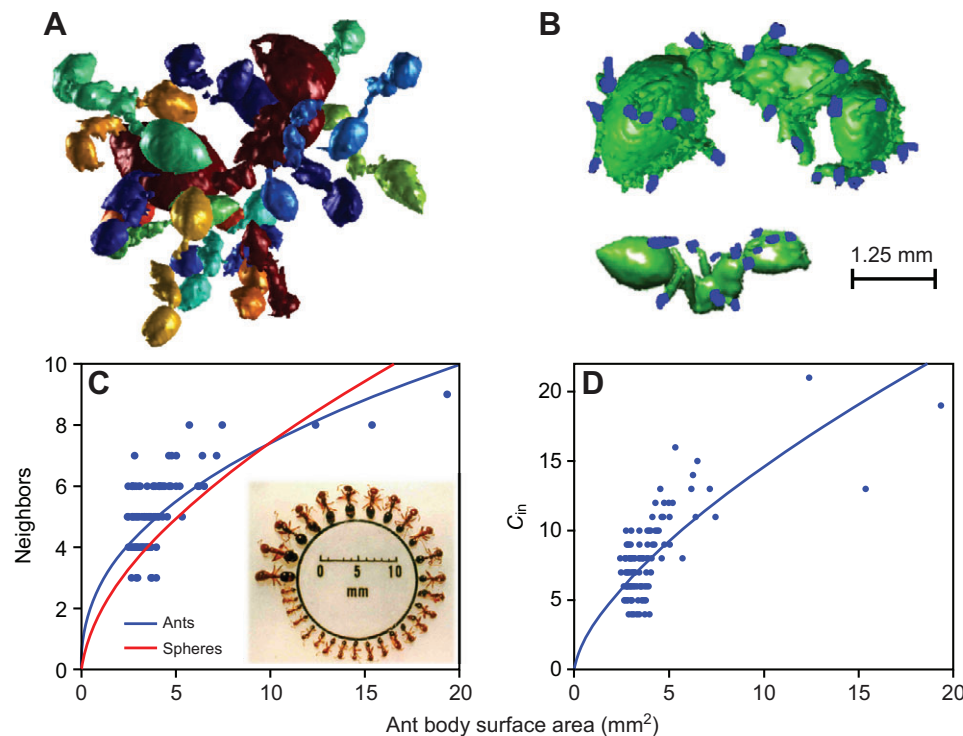


Fig. 6. The effect of body size on connectivity. (A) A large ant surrounded by and connected to many small ants. (B) Large and small single ants showing the high and low number of connections, respectively. (C) Relationship between an ant's body surface area and the number of neighbors to which it is connected. Best fit is a power law function with an exponent of 0.41 and $R^2=0.44$. The inset shows a polymorphism range within a single fire ant colony, reprinted with permission (Tschinkel, 2006). (D) Relationship between an ant's body surface area and the number of incoming connections it sees. Best fit is a power law function with an exponent of 0.35 and $R^2=0.53$. The low R^2 values for these models show that a large portion of the variation is unexplained by the models. We postulate that this is due not to an incorrect model but to high inherent scatter in the data (i.e. that the unexplained variation is random). To test this we averaged the data in 1 mm² bins and found the resulting R^2_{adjusted} values increased substantially to 0.84 and 0.87 for C and D, respectively, without noticeably changing the fits.

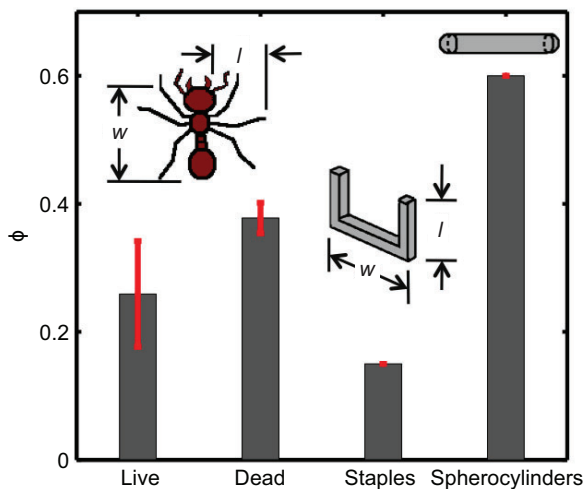


Fig. 7. Packing fraction (ϕ) for live and dead ants, staples and spherocylinders. Shown are mean and 95% confidence intervals of ϕ for live and dead ants (present study), staples (Gravish et al., 2012) and spherocylinders (Wouterse et al., 2007). All values are for body aspect ratios of $\alpha=4$. Ants halve packing fraction by using their legs to increase nearest neighbor spacing.

Live ants, with packing fraction $\phi_{\text{live}}=0.25\pm 0.05$, are packed 34% less tightly than dead ants, with a packing fraction $\phi_{\text{dead}}=0.38\pm 0.01$, as shown in Fig. 7. We verified the statistically significant increase by conducting a one-way nested ANOVA ($P<0.0001$, $F_{1,4}=1344$, $F_{4,42}=0.071$, $N_1=4\times 8$, $N_2=2\times 8$, variation between subgroups not significant at $\alpha=0.05$). This result is consistent with the ants actively using their legs to increase spacing between one another.

We found marked differences in packing fraction range between live and dead samples. Live samples yielded local packing fraction ϕ values ranging from 0.12 to 0.37 (four samples each with eight local subdivisions), but we did not find this spread for dead ant samples, whose packing fraction was relatively homogeneous, ranging from 0.37 to 0.4. The spread in live ant samples is likely due in part to large ants pushing harder against their neighbors than small ants, resulting in large voids and small voids, respectively.

Orientation correlation

To assess the relative orientation of ants, we introduced an orientation correlation metric. The orientation of a single ant may be described by a unit vector \mathbf{P}_1 pointing along the ant body's first principal moment of inertia as shown in Fig. 8A,B. Its first nearest

neighbor has orientation vector \mathbf{P}_2 . We define orientation correlation Ψ as the component of \mathbf{P}_2 in \mathbf{P}_1 's direction:

$$\Psi = \mathbf{P}_1 \cdot \mathbf{P}_2 = \cos \theta, \quad (2)$$

where θ is the angle between the two principal axis vectors. The angle θ between the vectors is limited to $0 \text{ deg} < \theta < 90 \text{ deg}$ because we were unable to algorithmically distinguish posterior from anterior of the ants in the scans; therefore, the limits of Ψ are 0 and 1. As Ψ nears zero, the ants are oriented more perpendicularly; approaching one indicates more alignment. A group of randomly oriented ants has an expected mean Ψ value of 0.5.

Fig. 8C shows the orientation correlation Ψ for live ants and dead ants. For live ants, $\Psi_{\text{live}}=0.44\pm 0.27$ indicating a slight tendency towards normal alignment, but a random packing of dead ants yields $\Psi_{\text{dead}}=0.6\pm 0.28$ showing a greater tendency towards parallel alignment. We verified the significance of the difference by comparing live and dead ants using a one-way nested ANOVA ($P=0.0015$, $F_{1,4}=58.1$, $F_{4,42}=0.863$, $N_1=4\times 110$, $N_2=2\times 110$, variation between subgroups not significant at $\alpha=0.05$). We also verified the difference from 0.5, the expected value for random orientation, finding both to be very significantly different with $P\leq 0.001$ (two-tailed one-sample t -tests: $N=440$, d.f.=439 for live ants, and $N=220$, d.f.=219 for dead ants; Bonferroni correction applied to t -tests to correct for multiple tests; sample pooling justified by lack of significant subgroup difference on nested ANOVA above).

DISCUSSION

In this study, we found evidence that ants actively control their arrangement within self-aggregations. This ability gives ant aggregations an intelligence and reacting ability greater than previously credited to them. To control their arrangement, ants likely require some degree of cooperation, the level of which remains unknown. Further investigation of ants actively rearranging their network may yield discovery of mechanisms for controlling arrangement and further inspiration for the development of biomimetic self-healing materials (Toohey et al., 2007).

Ants maintain spacing using active pushing of their legs

The spacing between ants is an important characteristic that determines the weight, porosity, buoyancy and water-repellency of the assemblage. The lighter a structure, the taller it can be built and the more easily it can be buoyed up to the water surface if submerged.

Our investigation of nearest neighbor distance and packing fraction, two parameters that vary inversely with one another, give both local and bulk views of spacing between ants. The initially

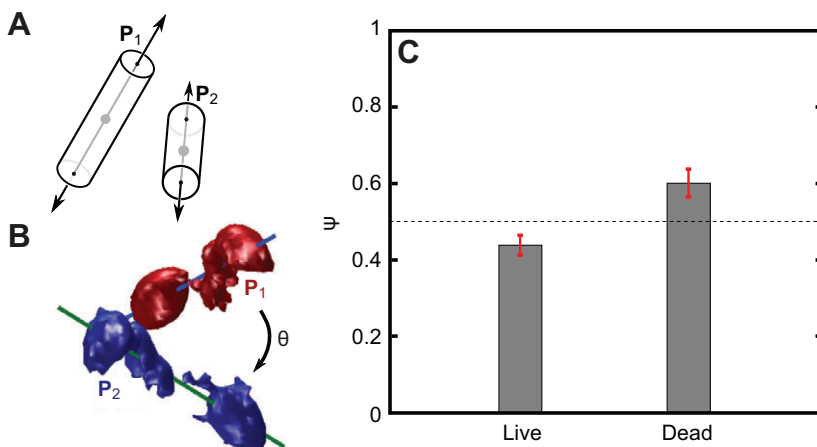


Fig. 8. Live ants orient themselves like T-junctions.

(A) Schematic diagram showing the \mathbf{P} vector, the axis running along an ant's principal moment of inertia. (B) Two neighboring ants with \mathbf{P} vectors shown. θ is the angle between the \mathbf{P} vectors. (C) Orientation correlation Ψ for live ($\Psi_{\text{live}}=0.44\pm 0.27$, mean \pm s.d.) and dead ($\Psi_{\text{dead}}=0.6\pm 0.28$) ants from this study. Live data are from four ant clusters with a total of 440 ants. Dead data are from two clusters with a total of 220 ants. An orientation correlation of 0.5 (dotted line) is expected from randomly oriented ants. Overall, live ants arrange themselves more perpendicularly to neighbors when compared with our control group of dead ants. Error bars show 95% confidence interval of the mean. Correlations of live and dead ants are statistically significantly different both from each other and from 0.5 with $P\leq 0.0001$. Published orientation results also show cylinders with aspect ratio $\alpha>1$ prefer parallel orientation (Bolhuis and Frenkel, 1997), which is consistent with the orientation of dead ants, but the opposite of that of live ones.

surprising result that first nearest neighbor distance is similar for live and dead ants, while second and higher are not, suggests that live ants are somewhat clustered or paired. This clustering makes sense because ant legs have a limited range of motion. Consequently, they are unable to push away neighbors positioned dorsally to them ('back to back'), but neighbors positioned anywhere else can be actively held at bay using their legs. While live ants can use their legs to push away most of their neighbors, they cannot push neighbors away that their legs cannot reach. Polymorphism may also play a role in the clustering, allowing small ants to actively fill gaps between larger neighbors. Although dead ants possess legs, they are unable to use them to make connections with neighbors or to push any neighbors away, as is done by live ants.

This difference is also apparent when comparing our results with simulations. When looking at the results for spherocylinders with aspect ratio $\alpha=4$ (ants have $\alpha=3.9\pm 0.17$), Wouterse et al. found a packing fraction ϕ of around 0.6, or more than twice that of live ants and 1.5 times that of dead ants ($\phi_{\text{live}}=0.25$ and $\phi_{\text{dead}}=0.38$) (Wouterse et al., 2007). Together, these differences show that the shape difference between spherocylinders and ants (including the presence of legs) is not solely responsible for the low packing density. Comparison of the dead and live ants shows that ants only achieve their minimum packing density when they are alive and able to actively hold themselves away from other ants.

Ants have six jointed legs which are mobile; staples are rigidly constructed U-shaped particles whose legs, or barbs, have no such mobility. Nevertheless, we compared staples with ants because the legs of both bring about new interaction dynamics between the particles relative to the spherocylinders. Studies of entangled staples also provide insight into the mechanism underlying the decreased packing fraction of live ants. Gravish et al. studied the geometrically induced cohesion of granular U-shaped particles, or staples (Gravish et al., 2012). They consider a dimensionless number Ω_{staples} to describe the barbs, the ratio of barb length l to spine length w (shown in Fig. 7). Despite ants having six legs, the analogous dimensionless number Ω_{ants} for ants is the ratio of leg length to body length, which is $\Omega_{\text{ants}}=l/w=0.73$ (shown in Fig. 7).

One of the key results of Gravish et al.'s study is that staples with longer barbs occlude their neighbors, which decreases packing fraction. Specifically, staples with the same leg-to-body length ratio as ants, $\Omega=7.3$, pack with $\phi=0.13$, half that of staples without barbs ($\phi=0.28$). This change is similar to that in our ant experiments, where live ants pack with $\phi=0.25$, significantly less than dead ants ($\phi=0.38$). From this comparison, we can again conclude that ants use their legs to reduce packing fraction.

Highly inter-connected networks

Ants display extraordinary strength, holding an average of 13 times their body weight in our observations of hanging columns of ants, and up to 400 times their body weight in tensile experiments between pairs of ants (Mlot et al., 2011). Such strength is needed in more natural situations as well. For example, consider a floating ant raft docking to a river bank to escape a flooded river; these linked ants are able to withstand being torn apart by the pull of turbulent currents. Our SEM results permit us to visualize and measure the connection mechanisms of the ant network that allows for such feats of strength.

Our investigations show that adhesive pad to tarsal connections are the most common attachments found in ant assemblages. These connections may account for the high elasticity or 'springy' feel to a cluster of linked ants, as they present more freedom of motion than adhesive pad to body- or mandible-based connections. This type of

connection likely affords the ants more room to bend their limbs to absorb impact or compressive forces.

In the context of granular materials, active attachment mechanisms such as adhesive pads and mandibles allow for compressive and tensile forces to be applied, providing a larger range of interactions than most granular materials. The importance of the active adhesive pad attachment in particular is shown by the ants' inability to self-assemble when their pads are deactivated by talc. Similarly, we observed that dead ants do not form stable aggregations, falling apart under their own weight when outside of a sample tube. This indicates that simple geometric entanglement, the only connection type in a dead assemblage, is insufficient to hold the structure together.

Our CT scan results provide quantitative insight into how the distribution of these connections differs from standard granular materials. For granular packing of most particles such as cylinders, contact results in compressive or frictional forces that support neighboring cylinders. Granular contacts cannot apply tensile stresses, such as those achieved by the ant network using tarsal pads.

Ants have a much higher density of contacts than comparably shaped granular materials. Through simulation, Philipse showed the contact number of packed spherocylinders asymptotically reaches $c=10$ as aspect ratio α is increased. The expected contact number of spherocylinders for an α matching our ants is 9 (Wouterse et al., 2009). Comparing this contact number with our measured result of 14.3 connections, it is clear that ants actively create many more connections than would be expected for equivalently shaped passive granular materials. Ants are able to exceed this theoretical limit for spherocylinders because they can use their legs to reach out to make connections with ants beyond those in their immediate vicinity as well as making redundant connections to the same neighbors. Fig. 5B shows a wide range in the distribution of connections per ant. As we discuss in the next section, this spread is also due in large part to the colony's polymorphism.

Polymorphism of the colony increases connectivity and packing fraction

Polymorphism in a colony results in more connections and tighter packing. Polymorphism refers to the large size distribution within a single fire ant colony, shown in the inset of Fig. 6C, where size is typically described by head width. Wood and Tschinkel found 45% of fire ant workers in a mature colony are small (head width up to 0.8 mm), 42% are medium (head width 0.8–1.0 mm) and 16% are large (head width greater than 1.0 mm) (Wood and Tschinkel, 1981). Despite this polymorphism, with some ants being more than 3 times larger than others, the aspect ratio ($\alpha=3.9\pm 0.17$) is preserved across scale. Another example of polymorphism is shown by our CT scan in Fig. 6A of ants with their legs digitally removed, where a large ant is surrounded by and connected to several small and medium-sized ants. The large size variation in a self-assemblage permits ants to achieve more connections and fit closer together, increasing the strength of the structure.

The effects of polymorphism are apparent in our result on connectivity. In Fig. 6D the largest ant is one of the most well connected to its neighbors, with 19 incoming connections, more than 4 times the connections seen by some of the smallest ants. Fig. 6B illustrates this point by comparing a large and small ant with both incoming and outgoing connections highlighted in blue. The large ant has many incoming connections all over its body and head, while the small ant has much fewer incoming connections.

In addition to having more connections, large ants have more neighbors than small ants. Fig. 6C shows that, as was the case for

our simulation with spheres, the number of neighbors does not scale linearly with ant size. The exponent for spheres appears somewhat higher than for ants, which we speculate is due in part to large ants being surrounded by a range of ant sizes, rather than a single size of smaller ant. Also, ant neighbors are counted by leg connections, not simply contacts as with spheres.

Ants in an assemblage are connected to anywhere from three to nine neighbors with the smallest ants connecting to the least neighbors. The largest ant was connected to nine different neighbors via 19 incoming connections, indicating that each neighbor is connected to it by an average of about two leg connections. The large size variation in a self-assemblage permits ants to fit closer together and achieve more connections, adding strength and redundancy to the structure.

Ants actively use all available leg connections

As fire ant connections are made actively, one can define a connective efficiency. Fire ants are remarkably good at finding connections with each other. Out of the 440 ants studied, 99% of them had all their legs completely attached to their neighbors. Only 26 legs remained dangling and unconnected, a very small percentage of the 2640 legs. As ants naturally try to keep all legs in contact with a surface when not moving, it is not surprising that the nearly static interior of the network is so well connected. We attribute the unconnected legs we found to either ants on the exterior of the assemblage or connections that may have been broken during sample preparation.

The high proportion of successful connections suggests that ants are indeed intent on maintaining grip with one another. The high connectivity adds strength to the aggregation, and is likely to be a common attribute between other insects such as bees and army ants able to form self-aggregations. Moreover, species of ants unable to form aggregations would likely have a lower connective efficiency.

Ants use their legs to orient themselves

Our results for the relative orientation of neighboring ants are surprising because they show that orientations between neighboring ants are not random. The orientation correlation of dead ants is consistent with studies of the orientation of spherocylinders (Bolhuis and Frenkel, 1997), indicating a tendency toward parallel alignment. However, live ants show the opposite effect, with a small but highly statistically significant tendency toward perpendicular orientation. From this we infer that ants actively behave in such a way as to position themselves perpendicular to each other. An active, randomly oriented motion of ants might be expected to lead to more randomized orientations, and thus values of orientation correlation closer to 0.5, but the observed value below 0.5 shows a non-random tendency toward perpendicular orientation.

The function, if any, of this behavior will require further investigation; however, we believe it may help with distribution of forces on the ant ball by redirecting incoming forces in different directions. If the orientation of ants within the aggregation were distributed truly randomly, it can be expected that there would be weak regions in the structure where several ants happen to line up, producing a potential fracture plane. Deliberately taking positions more perpendicular to neighboring ants would eliminate these regions.

A second possibility is that this behavior is designed to promote buoyancy of the aggregation. The reason that cylinders tend to orient parallel is that it increases the density of the aggregation (Bolhuis and Frenkel, 1997). Maintaining a perpendicular orientation thus

tends to decrease the density, and increase the buoyancy of the structure.

Another possibility is that the tendency may be geometric in origin. We have previously noted that ants in the back-to-back configuration cannot push against each other with their legs; however, consider the case where ants are actively attempting to walk forward: if the ants are parallel, they will tend to go past each other, but if they are perpendicular they will tend to collide, stopping the motion of at least one ant. The ant's approximately dumbbell shape will tend to enhance this interlocking effect. Thus, ants would tend to slow down when traveling perpendicular to their neighbors, spending more time in this configuration.

Ants as a biomaterial

This study also shows that fire ant aggregations share commonalities with well-known biomaterials. Namely, ant aggregations are porous, enabling them to be both lightweight and strong. Using porous materials has long been effective in making materials lighter without sacrificing strength. Porous aggregate concrete is known as a satisfactory substitute for lighter building material (Lo and Cui, 2004). Cancellous, or highly porous, bone is an excellent example of a naturally occurring porous network that is very strong. Cancellous bone with volume fractions as low as 0.03 and as high as 0.5 can withstand pressures of 1000 kPa and 100 MPa, respectively (Hernandez et al., 2001). Indeed, the ability to create porous structures in building materials is a trait common across scales and across species.

The effect of distribution of particle sizes has been studied in the context of granular media. In industrial applications, where space is an important factor, an increase in packing fraction means less wasted space. Granular studies have found that polydisperse packing has a higher packing fraction than monodisperse packing (Al-Raoush and Alsaleh, 2007). It is likely that a similar phenomenon occurs within ant aggregations as a result of colony polymorphism. We found in many instances that small ants tend to fill in spaces around large ants. While a lower packing fraction helps the colony stay afloat while rafting, efficient packing is equally important both to keep water from seeping in and to prevent weak spots in the raft. The experiments of Mlot et al. demonstrate the combination of high buoyancy and water impermeability created by this arrangement of live ants (Mlot et al., 2011). In theory, we might have been able to re-verify the buoyancy result in our fixed assemblages of ants. However, the hydrophilic property of the cyanoacrylate coating causes the assemblage to absorb water, preventing such a test.

Reproducibility of CT scans

Our study made use of a state-of-the-art 3D CT scanner which may not be available to other investigators. Nevertheless, methods such as visual inspection can yield important characteristics, such as ant spacing, which are consistent with those found using CT scanning. Using the ratio of the number of ants and their interpolated volume from our CT scans, we calculate an ant concentration of 164 ants cm^{-3} . Assuming a cubic lattice, the associated ant center-to-center spacing is 1.8 mm. Previously, by visual inspection of frozen ants in a raft, we found a planar concentration of 34 ants in 1 cm^2 (Mlot et al., 2011) and a spacing of 1.7 mm, a value quite close to our current findings based on CT scans. Thus, visual inspection of the surface of a self-aggregation can give a good indication of properties on the interior.

Future investigators may also be able to exceed certain limitations of our study based on the state of current technology. The size limitations in our CT scanning equipment set an upper bound of

scans at 150 ants. Such numbers are small compared with the size of most insect self-assemblages; for instance, fire ant rafts may number from 10,000 to 100,000 individuals (Mlot et al., 2012). So little is known about packing and order in these assemblages that it makes sense to choose the smallest assemblages. Also, instrumentation limitations do not allow scanning of samples of the size of those that occur naturally.

In addition, our small samples are further justified by our choice of species. Anderson rates insect self-assemblages in terms of complexity, with fire ants as the least complex self-assemblages, far less complex than weaver ant pulling chains and army ant tunnels and walls (Anderson et al., 2002). Thus, compared with other ant species, the arrangement of fire ants is less crucial to function. His view of assemblages suggests that our samples of fire ant self-assembly are good representations of the overall structure, despite their small size. Applying our CT scan technique to more sophisticated species such as army ants would require a CT machine capable of scanning a larger volume with a higher number of individuals.

The resolution of our CT scan prevents us from distinguishing an ant's anterior end from its posterior. Improvements to the technology will enable future workers to determine whether polarity is an important characteristic of the ant network. As we are unable to distinguish antennae from legs, and antennae do not contribute to the tensile integrity of the structure, they are excluded from our analysis (see Materials and methods, 'Calculation of measurements'). However, while antennae have no role in supporting tensile forces, they may be important in providing resistance to compressive stresses, as shown by the ability of ants to arrest falling in tunnels by extending their antennae (Gravish et al., 2013).

Conclusion

We measured the connectivity and arrangement of a 3D linked network of fire ants. Using micro-CT scanning we investigated the internal structure of these assemblages, which was not observable with previous methods. We found that ant aggregations are highly interconnected networks, possessing as much porosity as known biomaterials such as bone. We identified key ant behaviors that facilitate the formation of such porous, strong and responsive self-aggregations.

First, ants use their legs to extend the distance between neighbors. When ants increase the distance between one another with their legs, the raft becomes more porous and consequently buoyant. This trapping of air within the raft permits fire ant rafts to stay afloat and buoy back to the surface when submerged.

Ants also use their legs to arrange themselves into more perpendicular arrangements than observed in either their dead counterparts or randomly oriented spherocylinders with a similar aspect ratio. We speculate configurations in mutually perpendicular directions add to the adaptability of the structure, improving its resistance to fracture by environmental forces by redistributing loads in different directions.

Lastly, we found an important role in polymorphism of the colony, previously known to facilitate the colony in performing different tasks such as foraging, caring for the brood and defense. Here, such polymorphism plays an important role in increasing connectivity of the self-aggregation, relative to a colony of same-sized individuals.

Together, these properties make ant self-assemblages highly versatile tools enabling the colony to function successfully in a variety of situations. Local control of spacing may allow ants in a raft to keep water out even when submerged. Controlling orientation

may allow ants to build bridges and towers anisotropically, with greater strength in the direction of highest load. The high connectivity of the network evenly distributes forces among an ant's appendages, enabling an assemblage to support both static self-weight and dynamic external loads for long periods. These properties show that fire ant aggregations have higher levels of structural sophistication and active ordering than previously recorded.

MATERIALS AND METHODS

Environment setup

Ant husbandry

Three polygynous colonies of red imported fire ants (*S. invicta*) were procured from roadsides near Atlanta, GA, USA, during the summer of 2011. In selecting colonies, we aimed for an average ant mass of 1.5 mg by looking at average ant size. Colonies were removed from the soil, placed into bins, and cared for according to our previous methods (Mlot et al., 2011), and were fed crickets and water 3 times a week.

Sample preparation and imaging

Two methods were used to investigate the structure of ant aggregates: SEM imaging and micro-CT imaging. In both cases, ant aggregation was induced in live samples by placing ants in a container and moving the container in a horizontal swirling motion.

SEM imaging

A small group of about 15 live ants were confined to a Petri dish. The dish was swirled, inducing the ants to link together into a cluster against the side of the dish. The cluster was then flash frozen with liquid nitrogen before it could disassemble, and immediately gold-sputtered using a Cressington Sputter Coater 108 (Cressington Scientific Instruments, Watford, UK) and examined for intact connections using a Phenom G2 Pro Scanning Electron Microscope (Phenom World, Eindhoven, The Netherlands).

CT imaging

Two types of ant samples were prepared for CT scanning, live and dead, which we discuss in turn. Each sample was composed of 110 ants, the largest size that fit within our sample tubes. Here we describe our methods for moulding balls of ants, freezing them, and protecting them in cyanoacrylate vapor to protect them during the CT scanning process.

Four samples of 'live' ants were prepared, each containing 110 ants, for a total of $n_{\text{live}}=440$ ants. The schematic diagram in Fig. 9 demonstrates our methods for preparing live ant samples for CT scanning. To prepare the samples, we swirled a beaker containing 110 ants by hand. After 10 s of swirling, the ants produced a stable ball, which was then frozen by pouring liquid nitrogen into the beaker. The liquid nitrogen kills the insects instantly, but does not disturb the network structure, thereby preserving relative ant positions and the connections between ant legs. The frozen sample was then lightly coated with cyanoacrylate. Ethyl cyanoacrylate was boiled in a disposable aluminium pot over a small flame to produce cyanoacrylate vapor, as shown in Fig. 9. We found that aluminium was desirable because of its ability to inhibit polymerization of the cyanoacrylate. However, some polymerization did occur, requiring the pot to be replaced approximately every 90 s. The frozen ant ball was placed on a 7 mm wire mesh, and exposed to the cyanoacrylate vapor until a slight whitening was observed over the surface of the ball, indicating that a coating of cyanoacrylate had been deposited. During the coating process, the ball was kept frozen by applying liquid nitrogen roughly every 20 s. This coating prevented thawing induced settling, which can produce noisy images during the hours-long scanning process.

Two samples of 'dead' ants were prepared, each containing 110 ants, for a total of $n_{\text{dead}}=220$ ants. These samples consisted of a random arrangement of recently frozen individual ants. Ants were allowed to walk freely in a 13×13 cm container. The ants were flash frozen then allowed to thaw completely for 20 min. Any incidentally connected ants were carefully separated, before all the ants were placed into a CT scanning tube. The tube was shaken, allowing ant bodies to settle randomly. Dead ant samples did

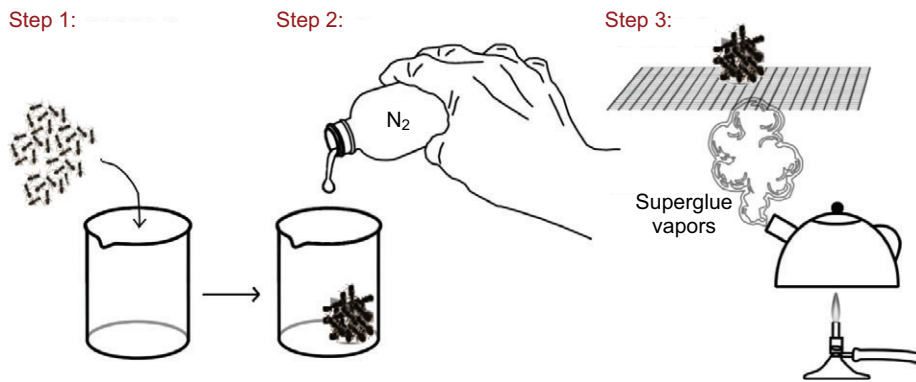


Fig. 9. Schematic diagram of the method used to prepare ant samples for scanning. Step one: collect ants in a beaker and induce ants to aggregate by swirling beaker. Step two: freeze ants with liquid nitrogen. Step three: preserve structure for scanning by coating with cyanoacrylate vapor.

not need to be coated with cyanoacrylate vapor because they were already thawed and did not move during scanning. We limited the time between freezing and scanning to 3 h to prevent desiccation and subsequent deforming of bodies.

Once the samples were prepared, both live and dead ants were scanned in the same fashion. Ant counts were made first by weighing; the counts were later verified using analysis of our CT scans and up to six ants were removed from the tops of some of the samples to keep 110 ants per sample. A sample was placed in a 14 mm diameter tube and scanned using a Scanco μ -CT 50 CT scan machine (Scanco Medical AG, Bruttisellen, Switzerland) with 7 μ m voxel size, 14 mm FOV, 2048 \times 2048 pixel matrix, E=55 kVp and I=200 μ A. Grayscale slice tomograms were converted to dicom format for further segmentation and image processing. Our CT scans produced thousands of images each representing a thin horizontal slice 7 μ m thick as shown in Fig. 3A. These scans were digitally stacked to produce a 3D rendering of the assemblage, as shown in Fig. 3B,C.

CT scan data processing

For all data processing we custom-wrote MATLAB algorithms designed to gather from the CT scan files the number of connected neighbors, connections per ant, packing fraction, orientation and neighbor spacing. Our algorithms distinguished body segments from appendages, assembled the bodies from segments, and traced the appendages from the bodies to find connections. Because of noise in the data, our algorithms sometimes failed to detect that touching body segments were distinct or grouped the segments into incorrect bodies. Our algorithms also sometimes associated appendages with the wrong ant by incorrectly deciding which side of a connection belonged to each ant. Before correction, 1.3% of connection points were incorrectly resolved, and 2.1% of body segments were incorrectly grouped or segmented. These mistakes are trivial for a human

reviewer to identify and were corrected by hand before calculating statistics. More details on the algorithms used can be found in the 'Additional methods' section below.

Calculation of measurements

Five major classes of measurements were compared in this work: connections per ant, number of connected neighbors, nearest neighbor distance, packing fraction and orientation correlation. All measurements are reported as means \pm s.d. In general, these were calculated directly from their definitions; however, special procedures were needed to deal with antennae and obtain standard deviations on the packing fraction measurements.

Because of algorithmic limitations, it was not possible to automatically distinguish antennae from legs, and it is very time consuming for a human to do so. However, we observed that the antennae almost always appeared with a slight gap between them and the surfaces they touched, meaning that they rarely registered as forming an incoming connection. However, they always registered as an outgoing connection, so in order to have our connection statistics count only structurally significant connections we simply forced $c_{out}=6$, with the assumption that the ant has all of its legs. In cases where more than six appendages appeared to touch something, the program asked to have the antennae manually deleted. Thus, there may have been a small number of errors where an antenna made contact and a leg did not, which would not trigger a manual review.

To measure local variability of packing fraction ϕ despite our small number of samples, we digitally divided each sample into eight parts at the principal planes. The principal planes are the three planes that result from placing the intersection of three orthogonal axes at the centroid of the sample. This procedure yielded a total of 32 parts for live samples and 16 for dead samples.

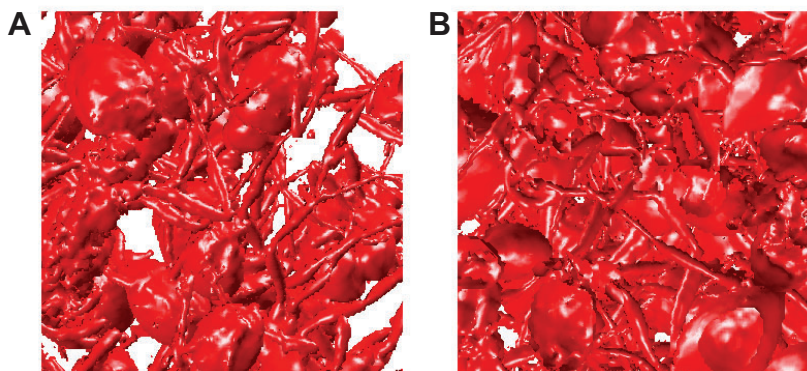


Fig. 10. The very high density of the dead ants causes problems for both automatic and manual tracing of connections. (A) A face-on view of a cube digitally cut from the center of a live ant assemblage. There is significant open space and both legs and bodies are clearly distinguishable, simplifying connection tracing and human verification. Some small amounts of noise are visible as floating blobs on the right of the image and surface bumps on the left, but they are easy to distinguish and remove. (B) An identically dimensioned cube cut from the center of a dead ant ball. There is little open space, and it is very hard to track connections through the clutter, either automatically or manually. The increased density also increases the noise in the reconstruction as a result of greater X-ray absorption, and the noise is also more likely to create a false connection or break a real one. Because of these difficulties, we were unable to measure connection-based metrics on the dead ant samples.

Comparison with simulations

We compared our results against other models of granular particles in the literature, including simulations of packing of spherocylinders and U-shaped particles with dimensions analogous to those of the ants in our study.

Wouterse et al. performed simulations of packed spherocylinders using the mechanical contraction method (Wouterse et al., 2007). Beginning with a sparse random configuration of non-overlapping particles, they dilated the particles step by step until no more iterations could be made without an overlap. We compared our packing fractions for ants with those obtained by Wouterse et al. for a similar body aspect ratio.

To gain insight into whether leg geometry influenced the packing fraction of ants, we looked at the studies of Gravish et al. (Gravish et al., 2012) on staple-shaped particles of analogous dimensions. We compared the effect of barbs on the packing of staples with the effect of legs on the packing of ants.

In order to investigate the effect of polymorphism (variation in ant size within a colony) on the number of connections, we also performed a 3D simulation of small spheres of varying radius, r , packing around a sphere of larger radius, R , with a similar distribution of radii, $1 < R/r < 3$, as our results for ant length. We measured the scaling of the number of contacts with surface area and compared this with our results for ants.

Measurement difficulties in dead ant samples

As shown in Fig. 10, the dead ant samples had increased density and homogeneity, and increased noise due to greater X-ray absorption, making it impossible to trace connections accurately or to verify the traced connections manually as was done in the live samples. Thus, no connection-based metrics (connection and neighbor counts) were obtainable. Nevertheless, we applied morphological opening, a standard image processing operation (Haralick and Shapiro, 1992), to remove the appendages from the sample and allow our algorithms to assemble ant bodies, so the body-based metrics (nearest neighbor distances and orientation correlation) were measured successfully. We also measured packing fraction, which is unaffected by the increased noise.

Statistical analysis

Throughout this work, we applied nested ANOVA tests to compare statistics from the live and dead ant sample groups, and to check for independence between samples of the same type (subgroups). In all cases there was no significant variation within subgroups. In the case where tests were carried out between the data and a theoretical value, t -tests were used with Bonferroni correction to correct for multiple tests. When fitting regressions to compare with simulations, we used regressions of the same form (power law) as those reported for the simulated case to allow for direct comparison.

Data processing

All data processing was done using MATLAB. Internal body cavities were filled in before further processing. Because 3D filling [using MATLAB's 3D *infill()* command] is very sensitive to small noise-induced holes in the body surface, we devised a noise-tolerant filling method. The principle is that if a point lies within a filled cavity then all slice planes through the point will contain a closed contour encircling the point. Because of noise, the contour may be broken in some of the slice planes, so for every point we sliced in 13 directions: the three directions orthogonal to coordinate axes (the cube faces), the six directions perpendicular to one axis and 45 deg to the others (the face diagonals), and the four directions at 45 deg to all axes (the octahedral faces). Encirclement in each plane was checked using MATLAB's 2D *infill()* command. We then accepted any point as an interior point if it was encircled in 10 or more of the slices.

Equivalent volume of the ball, V_i , was found by dilating [using MATLAB's *imdilate()* command] the ant ball until 95% of the interior was filled. Volume fraction was found by taking the ratio of the volume filled by ants, V_a , to total volume V_i . Ant balls were subdivided into eight quadrants and the method repeated on each quadrant to measure the variability of the volume fraction.

Ant bodies were labeled by eroding [using MATLAB's *imerode()* command] the data to remove limbs and find heads and gasters, which were then matched to form ant bodies. The matching process was semi-automated, with all matching checked by hand.

An ant's connection count was defined as the sum of the number of non-intersecting two-ant connections that touch its body, assigned multi-ant connections (defined below), and connections that did not terminate (i.e. a leg or antenna that contacts no other ant). Two-ant connections were defined as any filled region connecting exactly two ant bodies. Multi-ant connections occurred relatively frequently, usually where a leg made grazing contact with an ant on the way to another ant or where two appendages touched the same ant body and each other. In these cases, an attempt was made to remove the grazing contact or convert the multi-ant connection into several two-ant connections. First the bodies were dilated by twice the maximum leg diameter. If this procedure broke the jumble of legs into a pair of two-ant connections, the contact with the ant body closest to the centroid of the break was considered a grazing contact and discarded, with the remaining ants assigned one connection each. If the connection did not break, it was assumed to be the case where several appendages from multiple ants were touching. To attempt to convert this to several two-ant connections the bodies of the ants involved were dilated as much as possible without causing them to touch and then the connections recounted. If this still failed, the ants were assigned connections according to the number of unique contacts made between the connection and each ant body.

Because of algorithmic limitations, it was not possible to automatically distinguish antennae from legs, and it is very time consuming for a human to do so. However, we observed that the antennae almost always appeared with a slight gap between them and the surfaces they touched, meaning that they rarely registered as forming an incoming connection. However, they always registered as an outgoing connection, so in order to have our connection statistics count only structurally significant connections, we simply forced $c_{out}=6$, with the assumption that the ant has all of its legs. In cases where more than six appendages appeared to touch something, the program asked to have the antennae manually deleted. Thus, there may have been a small number of errors where an antenna made contact and a leg did not, which would not trigger a manual review.

Assumptions of statistical tests

This work used nested ANOVA and t -tests. These tests require that the sampling distribution of the sample (and subsample for nested ANOVA) means are normally distributed, and that the variance is chi-squared distributed. The latter assumption is typically omitted for sample or subsample sizes greater than 30, as the tests are insensitive to the variance distribution at this size.

For the tests on neighbor- and connection-based statistics, the large subsample size of 110 ants per aggregation allowed us to invoke the central limit theorem to satisfy the requirement for normality of the sample mean. The central limit theorem in turn requires that the data are identically distributed and independent. One of the core assumptions of this work is that ant aggregations possess only short-range order, and thus while the data may be correlated over short distances, each datum is pairwise independent of most of the other data in the aggregation. To check this assumption, we inspected normal quantile plots of sample means drawn from 100,000 bootstrap samples of the data for each test, which showed good linearity, suggesting that the sampling distribution of the sample mean is approximately normally distributed.

For the packing fraction data, it was necessary to assume that the data were approximately normally distributed within each subsample because there were only eight parts per subsample. This assumption was reasonable because packing fraction is a spatial average, and thus tends to be normally distributed in materials exhibiting no long-range order. Normality of the data implies normality of the mean and chi-squared variance, satisfying the required assumptions for the tests. We checked empirically for normality of the data by looking at normal quantile plots of the combined data set of all pieces within each sample, which appeared linear and thus normal. Thus, we have empirically checked the condition for the part of the nested ANOVA that we were most concerned with, the test for equality of sample means. Each individual subsample did not contain enough data to tell from the normal quantile plots whether the data were normally distributed or not.

Acknowledgements

The authors thank R. Gummedi for his early contributions and N. Gravish for his insight and direction. Niles Lund provided artwork used in Fig. 9 by permission.

Competing interests

The authors declare no competing financial interests.

Author contributions

P.C.F. developed the cyanoacrylate fixation technique, helped with experiments, wrote software and did analysis and statistics on the data, developed the new measurement metrics used in this work, as well as wrote the final version of the paper. N.J.M. performed experiments, obtained and maintained ant colonies, wrote the first version of the paper, and identified connections to outside work in other fields. A.L. performed micro-CT scanning and provided significant expertise needed to both obtain the data and design the experiments to work with the available equipment. D.L.H. provided ideas, quality control, and editing of the manuscript.

Funding

This work was supported by the US Army Research Laboratory and the US Army Research Office Mechanical Sciences Division, Complex Dynamics and Systems Program, under contract number W911NF-12-R-0011.

Supplementary material

Supplementary material available online at
<http://jeb.biologists.org/lookup/suppl/doi:10.1242/jeb.093021/-/DC1>

References

- Al-Raoush, R. and Alsaleh, M.** (2007). Simulation of random packing of polydisperse particles. *Powder Technol.* **176**, 47-55.
- Anderson, C. and McShea, D. W.** (2001). Intermediate-level parts in insect societies: adaptive structures that ants build away from the nest. *Insectes Soc.* **48**, 291-301.
- Anderson, C., Theraulaz, G. and Deneubourg, J. L.** (2002). Self-assemblages in insect societies. *Insectes Soc.* **49**, 99-110.
- Blouwoff, J. and Fraden, S.** (2006). The coordination number of granular cylinders. *Europhys. Lett.* **76**, 1095.
- Bolhuis, P. and Frenkel, D.** (1997). Tracing the phase boundaries of hard spherocylinders. *J. Chem. Phys.* **106**, 666-687.
- Bonabeau, E., Theraulaz, G., Deneubourg, J.-L., Lioni, A., Libert, F., Sauwens, C. and Passera, L.** (1998). Dripping faucet with ants. *Phys. Rev. E* **57**, 5904.
- Cully, S. and Seeley, T.** (2004). Self-assemblage formation in a social insect: the protective curtain of a honey bee swarm. *Insectes Soc.* **51**, 317-324.
- Desmond, K. and Franklin, S. V.** (2006). Jamming of three-dimensional prolate granular materials. *Phys. Rev. E* **73**, 031306.
- Donev, A., Cisse, I., Sachs, D., Variano, E. A., Stillinger, F. H., Connelly, R., Torquato, S. and Chaikin, P. M.** (2004). Improving the density of jammed disordered packings using ellipsoids. *Science* **303**, 990-993.
- Gravish, N., Franklin, S. V., Hu, D. L. and Goldman, D. I.** (2012). Entangled granular media. *Phys. Rev. Lett.* **108**, 208001.
- Gravish, N., Monaenkova, D., Goodisman, M. A. and Goldman, D. I.** (2013). Climbing, falling, and jamming during ant locomotion in confined environments. *Proc. Natl. Acad. Sci. USA* **110**, 9746-9751.
- Groß, R. and Dorigo, M.** (2008). Self-assembly at the macroscopic scale. *Proc. IEEE* **96**, 1490-1508.
- Haralick, R. and Shapiro, L.** (1992). *Computer and Robot Vision*. Reading, MA: Addison-Wesley.
- Hernandez, C. J., Beaupré, G. S., Keller, T. S. and Carter, D. R.** (2001). The influence of bone volume fraction and ash fraction on bone strength and modulus. *Bone* **29**, 74-78.
- Lioni, A., Sauwens, C., Theraulaz, G. and Deneubourg, J.-L.** (2001). Chain formation in *Oecophylla longinoda*. *J. Insect Behav.* **14**, 679-696.
- Lo, T. and Cui, H.** (2004). Effect of porous lightweight aggregate on strength of concrete. *Mater. Lett.* **58**, 916-919.
- Mlot, N. J., Tovey, C. A. and Hu, D. L.** (2011). Fire ants self-assemble into waterproof rafts to survive floods. *Proc. Natl. Acad. Sci. USA* **108**, 7669-7673.
- Mlot, N., Tovey, C., and Hu, D.** (2012). Dynamics and circularity of large fire ant rafts. *Commun. Integr. Biol.* **5**, 590-597.
- Schneirla, T. C.** (1971). *Army Ants: A Study in Social Organization*. San Francisco, CA: W. H. Freeman.
- Theraulaz, G., Bonabeau, E., Sauwens, C., Deneubourg, J.-L., Lioni, A., Libert, F., Passera, L. and Solé, R.** (2001). Model of droplet dynamics in the Argentine ant *Linepithema Humile* (Mayr). *Bull. Math. Biol.* **63**, 1079-1093.
- Toohy, K. S., Sottos, N. R., Lewis, J. A., Moore, J. S. and White, S. R.** (2007). Self-healing materials with microvascular networks. *Nat. Mater.* **6**, 581-585.
- Tschinkel, W. R.** (2006). *The Fire Ants*. Cambridge, MA: Belknap Press.
- Wood, L. A. and Tschinkel, W. R.** (1981). Quantification and modification of worker size variation in the fire *Antsolopsis invicta*. *Insectes Soc.* **28**, 117-128.
- Wouterse, A., Williams, S. R. and Philipse, A. P.** (2007). Effect of particle shape on the density and microstructure of random packings. *J. Phys. Condens. Matter* **19**, 406215.
- Wouterse, A., Luding, S. and Philipse, A.** (2009). On contact numbers in random rod packings. *Granular Matter* **11**, 169-177.
- Zhao, J., Li, S., Zou, R. and Yu, A.** (2012). Dense random packings of spherocylinders. *Soft Matter* **8**, 1003-1009.